Analysis and Reliability Evaluation of a High Step-Up Soft Switching Push–Pull DC–DC Converter

Hadi Tarzamni ⓘ , *Student Member, IEEE*, Ebrahim Babaei ⓘ , *Senior Member, IEEE*, Farhad Panahandeh Esmaeelnia,
Payman Dehghanian ⓘ , *Member, IEEE*, Sajjad Tohidi, and Mohammad Bagher Bannae Sharifian

Abstract—In this article, a new soft switching isolated push–pull dc–dc converter using a three-winding transformer is proposed. The proposed hybrid resonant and pulse width modulated converter employs a conventional push–pull structure in the primary side, a voltage doubler in the secondary side, and a bidirectional switch besides the transformer, altogether help offering a high efficiency over a wide range of input and output voltage signals with an unsophisticated fixed-frequency control mechanism. The primary-side switches are commutated under zero voltage switching with low switching current and the secondary-side diodes are commutated under zero current switching. In this article, we first present an in-depth analysis of various operation modes and design constraints. Our analysis is further complemented with a comprehensive reliability evaluation of the proposed converter under various short circuit and open circuit fault scenarios. Different from the previous research, the derated operating states of the proposed converter are detailed and characterized in the reliability evaluations. A comparison study is then provided to evaluate the performance of the proposed converter against other similar converters from the operation, components count, efficiency, and reliability perspectives. Finally, the theoretical analyses are verified via tests and experiments performed on a 280 W/34.7 kHz prototype.

Index Terms—Faults, mean time to failure (MTTF), open circuit (OC), reliability analysis, short circuit (SC), soft switching isolated push–pull dc–dc converter.

I. INTRODUCTION

ISOLATED dc–dc converters have been widely utilized in renewable energy systems, electric vehicles, aircrafts, and home appliances, such as power conditioning systems [1], [2].

The growing demand for such technologies and the intensified economic constraints in the electric industry calls for advanced mechanisms enabling efficient and low-cost designs of dc–dc converters [3]. One simple-in-control and low-in-cost class of isolated dc–dc converters is the conventional pulse width modulated (PWM) flyback dc–dc converter [4]. While cost effective with a relatively low number of components, they lack a capability for direct power transfer to the load. Some other classes of flyback converters are recommended in response, such as quasi-resonant flyback converters [5], active clamp flyback converters [6], and full soft switching flyback converters [7], to enhance the operation efficiency, but at the cost of additional number of components and sophisticated control systems.

Series resonant converters operating with direct power transfer from input source to the load, soft switching of semiconductors, and reasonably good magnetic utilization are one of the most efficient isolated-type dc–dc converters. In [8] and [9], a class of series resonant converters is recommended, where the resonant tanks help ensure that the switches turn OFF under zero current switching (ZCS) conditions. While this practice offers a higher operation efficiency, they are still bulky. In the other related literature, ZCS techniques are proposed and applied using active auxiliary cells, in which sophisticated cells and control systems are employed to commutate the switches under ZCS conditions. For instance, in [10], two auxiliary active switches are utilized in the auxiliary cell. In [11], an *LLC* isolated resonant converter is presented, in which the input voltage regulation and a high efficient operation are achieved over a very limited range. In [12], an optimized wide-range *LLC* converter is introduced, in which the operation far from the resonant frequency leads to larger circulating current and, hence, poor efficiency. In [13], one modified *LLC* converter is presented where high efficiency is achieved over a wide range of input voltage, but reveals a poor operation under light-load scenarios.

Push–pull dc–dc converters are the other popular class of isolated converters. In order to improve the operation efficiency in this class of isolated dc–dc converters, several soft switched topologies are introduced in the literature. In [14], a zero voltage and ZVS (ZVZCS) push–pull converter is presented, in which the primary-side switches are commuted under ZVZCS conditions, whereas the secondary-side diodes are still hard switched. In [15], a current-fed ZVZCS push–pull converter is presented, which provides zero voltage switching (ZVS) and ZCS for the primary- and secondary-side semiconductors, respectively. In [16] and [17], two ZVS push–pull converters are suggested,
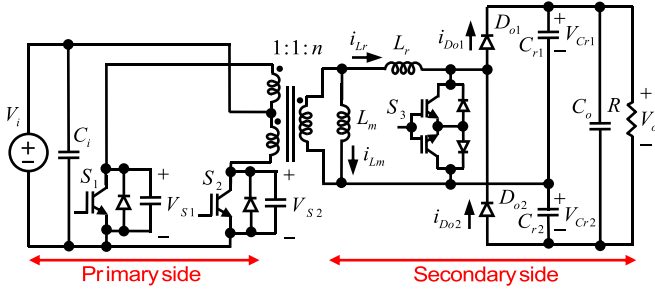
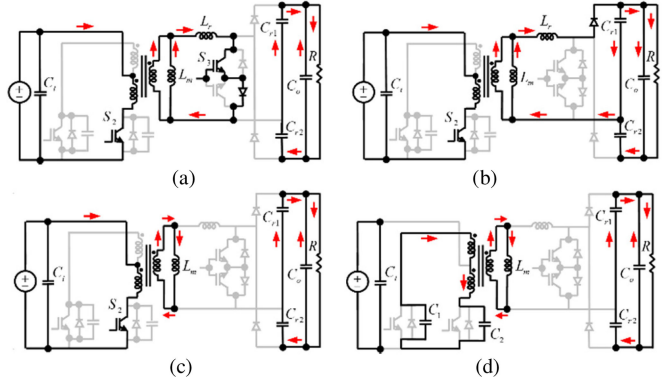Fig. 1. Proposed soft switching isolated push–pull dc–dc converter.

Fig. 2. Operational modes of the proposed converter. (a) Mode 1. (b) Mode 2. (c) Mode 3. (d) Mode 4.

Fig. 3. Steady-state key waveforms of the converter operation.

where ZVS of the primary-side switches is achieved, while still prone to the switching losses in the secondary-side semiconductors. In [18]–[20], several other topologies for soft switching push–pull converters are presented, where soft switching of the main switches is provided to reduce the switching loses. Majority of these topologies are, however, bulky—with a large number of semiconductors and intensified conduction losses.

Several research efforts can be found in the literature that evaluate the converters performance under different operating conditions and from different perspectives, e.g., reliability and mean time to failure (MTTF). In [21] and [22], the reliability performance of the interleaved PWM boost converters is assessed and compared with that of single-stage conventional boost converter. In [23], an interleaved full soft switching dc–dc boost converter is presented and its reliability performance is compared with that of the single-stage soft switching and hard switching boost converters. In [24], a conventional buck–boost converter is evaluated from reliability and MTTF points of view.

In this article, a new soft switching isolated push-pull dc–dc converter is introduced characterized with a simple resonant system, where ZVS and ZCS are achieved in the primary-side switches and secondary-side diodes, respectively. We analyze the reliability performance of the proposed converter by characterizing its derated operating states under a variety of operation conditions and short circuit (SC)/open circuit (OC) fault scenarios. Reliability performance comparisons against the similar class of converter topologies are conducted. Eventually, the proposed converter is experimentally tested with extensive analysis to verify its operational and reliability performance.

II. PROPOSED CONVERTER VERSUS STATE-OF-THE-ART PUSH–PULL CONVERTERS

The proposed soft switching push–pull dc–dc converter is demonstrated in Fig. 1. It contains two switches (S_1 and S_2) of a push–pull structure in the primary side, two diodes (D_{o1} and D_{o2}) and two capacitors (C_{r1} and C_{r2}) in the secondary side, one bidirectional switch (S_3) and a three-winding transformer with turns ratio of n, a magnetizing inductor (L_m), and a leakage inductor (L_r). Furthermore, one filter capacitor (C_o) is placed in the output load terminal. Capacitors C_{r1} and C_{r2} establish a voltage doubler with D_{o1} and D_{o2} diodes in the secondary side and also a resonant tank with inductance L_r. The following assumptions are considered here to simplify the operation mode analysis of the proposed converter [25]–[27].
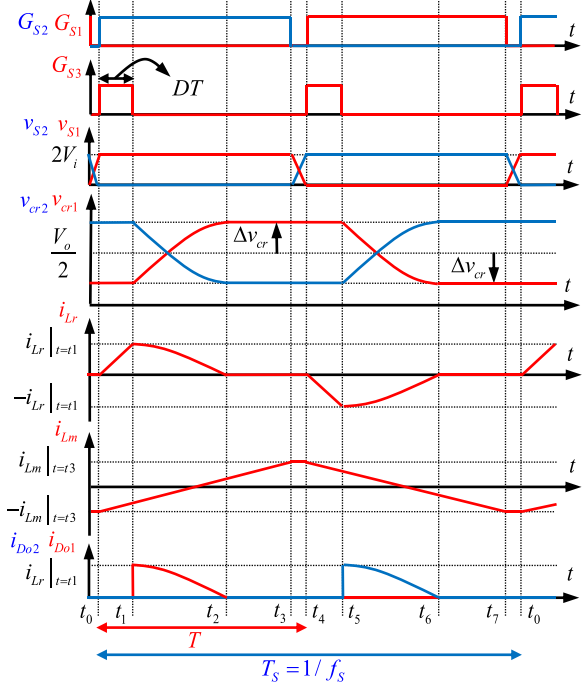
1) All components and devices are assumed ideal.
2) The input voltage V_i is assumed constant.
3) The output filter capacitor C_o is assumed large enough to be considered with constant output voltage V_o.
4) The C_{r1} and C_{r2} capacitors are assumed equal, expressed by C_r.
5) The capacitance of C_o is much larger than the capacitances of C_{r1} and C_{r2}.
6) The nonideal transformer is modeled by an ideal transformer with the inductances of L_m and L_r.

The proposed converter operates in four different operation modes in a half switching cycle, where the other four modes of operation are repeated symmetrically in the next half. The current flow paths of these operation modes are illustrated in Fig. 2 and the steady-state key waveforms are provided in Fig. 3.

Mode 1 $(t_0 \leq t < t_1)$: This operation mode starts when switches S_2 and S_3 are turned ON, resulting in the V_i voltage across each primary winding of the transformer. Prior to this mode, the current (i_{Lr}) flowing through the inductor L_r is zero and the voltage (v_{Cr1}) across the capacitor C_{r1} is at its minimum. Since the output voltage is twice v_{Cr1}, the initial condition for v_{Cr1} can be characterized as follows:

$$v_{Cr1}\,|_{t=t_0} = v_{Cr1}\,|_{\min} = \frac{V_o}{2} - \Delta v_{Cr} \tag{1}$$

where Δv_{Cr} is the voltage ripple across C_{r1} and is equal to

$$\Delta v_{Cr} = \frac{P_o T}{2 V_o C_r} \tag{2}$$

where T is the half switching cycle in the proposed converter and is approximately equal to $t_3 - t_0$ or $t_7 - t_4$, and P_o is the output power. As formulated in (3) and (4), i_{Lm} and i_{Lr} increase linearly with the nV_i voltage in this operation mode, which is similar to the conventional PWM boost converter, given by

$$i_{Lm} = \frac{nV_i}{L_m}(t - t_0) + i_{Lm}\,|_{t=t_0} \tag{3}$$

$$i_{Lr} = \frac{nV_i}{L_r}(t - t_0) \tag{4}$$

where the initial condition for i_{Lm} is enforced in the following equation taking into account the symmetrical observations in its waveform at $t = t_0$ and $t = t_4$:

$$i_{Lm}\,|_{t=t_0} = \frac{-nV_i T}{2L_m}. \tag{5}$$

Mode 2 $(t_1 \leq t < t_2)$: At $t = t_1$, the switch S_3 is turned OFF, whereas switch S_2 is still ON, transferring the input power to the output load through diode D_{o1}. In this mode, the inductor L_r and the parallel combination of C_{r1} and C_{r2} capacitors resonate. The initial conditions in operation mode 2 are evaluated as follows:

$$i_{Lm}\,|_{t=t_1} = \frac{nV_i(2D-1)T}{L_m} \tag{6}$$

$$i_{Lr}\,|_{t=t_1} = \frac{nV_i DT}{L_r} \tag{7}$$

where DT is a parameter representing the ON-time duration of the S_3 bidirectional switch in the operation mode 2 and controls the output power with fixed frequency in maximum power point tracking applications. The main resonant equations in this operation mode are formulated as follows:

$$i_{Lr} = i_{Do1} = \frac{r}{Z_r} \sin[\theta_1 - \omega_r(t - t_1)] \tag{8}$$

$$v_{Cr1} = v_{S3} = nV_i + r\cos[\theta_1 - \omega_r(t - t_1)] \tag{9}$$

where ω_r and Z_r are the resonant angular frequency and characteristic impedance of the resonance between L_r and the parallel combination of C_{r1} and C_{r2}, respectively, and are determined as follows:

$$\omega_r = 2\pi f_r = \frac{1}{\sqrt{L_r(C_{r1} + C_{r2})}} \tag{10}$$

$$Z_r = \sqrt{\frac{L_r}{C_{r1} + C_{r2}}}. \tag{11}$$

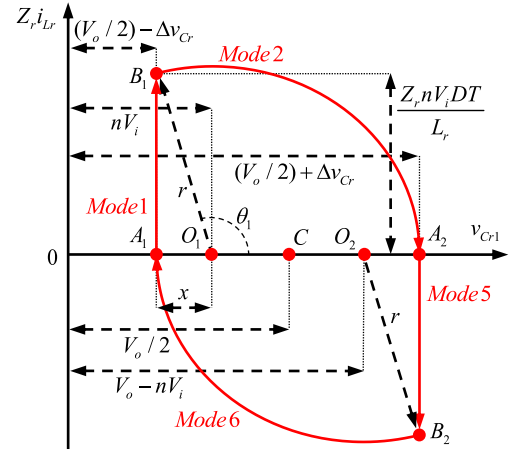

Fig. 4.   Resonant tank trajectory.

Then, the r and θ_1 parameters are obtained as follows:

$$r = \frac{V_o}{2} + \Delta v_{Cr} - nV_i \tag{12}$$

$$\theta_1 = \cos^{-1}\left(\frac{r - 2\Delta v_{Cr}}{r}\right). \tag{13}$$

The preceding equations are concluded from the resonant tank trajectory of the state variables, demonstrated in Fig. 4 and fully described in Section III.

Mode 3 $(t_2 \leq t < t_3)$: At $t = t_2$, the diode D_{o1} turns OFF under ZCS condition and no power is transferred from the input source to the output load. This operation mode is employed to ensure the ZCS condition for the secondary-side diodes. Since the proposed converter always operates at a fixed frequency $(f_S = 1/2T)$ at a range close to the series resonant frequency $(f_r = \omega_r/2\pi)$, the i_{Lm} current is always small and the primary-side switches commutate under a low switching current. The current flowing in the primary-side switch (i_{S2}) at the end of this operation mode is evaluated as follows:

$$i_{S2}\,|_{t=t_3} = \frac{n^2 V_i T}{2L_m}. \tag{14}$$

In this mode, the v_{Cr1} voltage is in its maximum as follows:

$$v_{Cr1}\,|_{t=t_2} = v_{Cr1}\,|_{t=t_3} = \frac{V_o}{2} + \Delta v_{Cr}. \tag{15}$$

Mode 4 $(t_3 \leq t < t_4)$: At $t = t_3$, the switch S_2 is turned OFF and the i_{Lm} current is at its maximum (I_{Lm}). As this operation mode is very short, it can be presumed as a current source, where the current flows through the parasitic capacitors of the primary-side switches, charging C_2 and discharging C_1 capacitors linearly. Operation mode 4 can be characterized through the following equations:

$$I_{Lm} = \frac{nV_i T}{2L_m} \tag{16}$$

$$v_{s1} = 2V_i - \frac{nI_{Lm}}{2C_1}(t - t_3) \tag{17}$$

$$v_{s2} = \frac{nI_{Lm}}{2C_2}(t - t_3) = \frac{n^2 V_i T}{4L_m C_2}(t - t_3). \tag{18}$$

Refs.	Number of Switches	Number of Diodes	Number of Capacitors	Number of Inductors	Primary-Side Switches (Diodes)	Secondary-Side Switches (Diodes)	Transformer Turns Ratio	Duty Cycle	Voltage Gain
Proposed	3	2	3	0	ZVS	ZCS	4:4:50	40%	28
[14]	2	4	2	0	ZVZCS	Hard	2:2:36	48%	15.7
[15]	2	4	2	1	ZVS	ZCS	1:1:35	46%	33.3
[16]	2	4	1	1	ZVS	Hard	1:1:21	N.P.	19.5
[17]	2	4	2	2	ZVS	Hard	N.P.	47%	6.1
[18]	6	0	1	1	ZVS	ZCS	1:1:10	80%	25
[19]	9	0	2	1	Hard	ZVS	1:8	75%	7.9
[20]	8	0	4	2	ZVS	ZCS	26:26:48	80%	9

N.P.: Not provided.

With a short time interval described in (19), the operation mode 4 ends when v_{S1} reaches zero at $t = t_4$. This is when the S_1 switch can be turned ON under ZVS condition in the second-half switching cycle

$$t_4 - t_3 = \frac{4L_m C_2}{n^2 T}. \tag{19}$$

At $t = t_4$, one half of the switching cycle ends and the second half starts with S_1 switch turned ON.

A comparison study on the operation of the proposed push–pull topology and the state-of-the-art push–pull converters is presented in Table I. The comparison is provided with regard to several factors including the number of elements, the soft switching conditions, and the voltage boost capability of the converters. Comparison results demonstrate the operation superiority of the proposed converter. According to Table I, the proposed converter assembles five semiconductors, which is lower than the competitors. Furthermore, the proposed converter topology offers soft switching transitions for both primary- and secondary-side semiconductors, similar to those suggested in [15], [18], and [20]. Considering the duty cycle and transformer turns ratio requirements, the proposed topology reveals an acceptably high voltage gain among other topologies in the literature.

III. RESONANT TANK TRAJECTORY

In order to simplify the operational mode analysis of the proposed push–pull converter, its resonant tank trajectory including state variables of i_{Lr} and v_{Cr1} is presented in Fig. 4. As the converter starts its operation in one switching cycle ($t = t_0$), the converter's operating point is at A_1 with $i_{Lr} = 0$ and the minimum v_{Cr1}. During operation mode 1, the operating point transits from A_1 to B_1 with linear increase in i_{Lr} and under a constant v_{Cr1}. In operation mode 2, the operating point moves from B_1 to A_2 on a circular path characterized by the resonance between L_r and the parallel combination of C_{r1} and C_{r2}. The center point of this circular path is O_1, which is located at $(nV_i, 0)$ with the radius r—see (12). θ_1 is the angle formed by the initial conditions in operation mode 2—see (13). The duty cycle corresponding to switch S_3 (D) is assessed using the Pythagorean theorem on $A_1 B_1 O_1$ triangle

as follows:

$$\left(\overline{A_1 B_1}\right)^2 = \sqrt{r^2 - x^2} \tag{20}$$

$$x = nV_i - \frac{V_o}{2} + \Delta v_{Cr} \tag{21}$$

$$D = \frac{1}{nV_i} \sqrt{\frac{2L_r P_o}{T} \left(1 - \frac{2nV_i}{V_o}\right)}. \tag{22}$$

The preceding equations demonstrate that D depends on both n and P_o. Since D is small under most operating conditions, direct power transfer is achieved in the proposed converter during most of the switching cycle duration. During operation modes 3 and 4, i_{Lr} and v_{Cr1} are constant. Therefore, the trajectory path stays around the operating point A_2. This continues until operation mode 4 ends, when the second half cycle starts from A_2 with a symmetrical path transmission.

IV. RELIABILITY ANALYSIS AND PERFORMANCE EVALUATIONS

This section elaborates the reliability assessment of the proposed push–pull converter centered on the Markov process models. The reliability analytics proposed in this research trail the following procedure:

1) characterization of the converter operating states under different fault scenarios;
2) Markov chain process for both SC and OC fault scenarios;
3) components' failure rate assessments in each operating state considering the nonideal operation characteristics;
4) quantification of the reliability and MTTF metrics under both SC and OC fault scenarios;
5) assessment of the system overall reliability performance.

The converter's operating states under different SC and OC fault scenarios on the components are first determined. Any SC fault scenario on the proposed converter topology results in the total system failure, represented as the *absorbing state*. Under OC fault scenarios on some components, however, the converter continues to function in other operating states with different power flow arrangements, represented as *derated states*. The introduced operating states are demonstrated in Fig. 5 and their specifications are indicated in Table II. As indicated in Table II, the OC faults on S_1 or S_2 switches, S_3 switch, and C_{r1} or C_{r2} capacitors will change the converter operating state similar
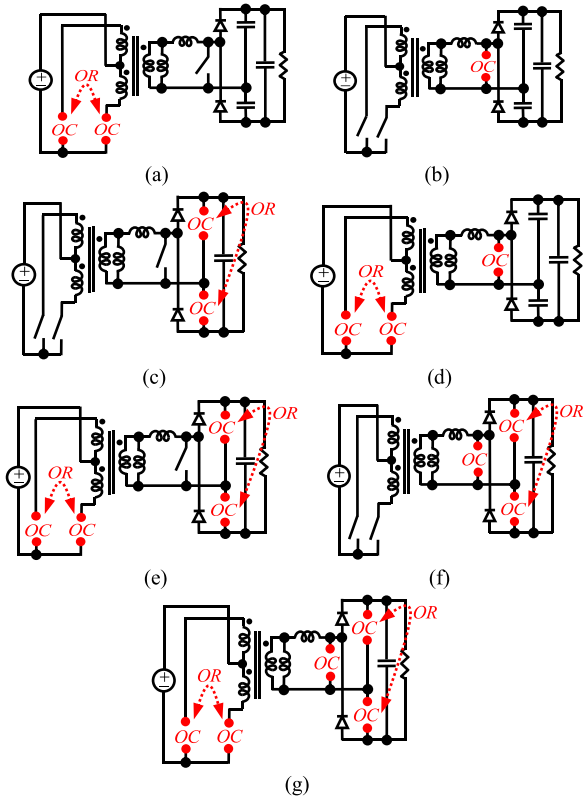
Fig. 5. Converter's different operating states under OC fault scenarios. (a)–(g) correspond to the OC fault operating states of 2–8 in Table II.

TABLE II
SPECIFICATIONS OF DIFFERENT OPERATING STATES UNDER OC FAULT SCENARIOS

State #	Condition	OC Fault on Components	Specification
1	Full power	-	Healthy (Initial State)
2		S_1 or S_2	Soft Switching Flyback
3		S_3	Hard Switching Push-Pull
4		C_{r1} or C_{r2}	Asymmetric Soft Switching Push-Pull
5	Derated Power States	S_1 or S_2, and S_3	Hard Switching Flyback
6		S_1 or S_2, and C_{r1} or C_{r2}	Asymmetric Soft Switching Flyback
7		S_3, and C_{r1} or C_{r2}	Asymmetric Hard Switching Push-Pull
8		S_1 or S_2, and C_{r1} or C_{r2}, and S_3	Asymmetric Hard Switching Flyback
9	No Power	-	Total Failure (absorbing state)

to that observed in flyback converters, hard switching, and asymmetric operations, respectively.

With the operating states identified, the Markov chain architecture corresponding to the proposed converter under SC and OC fault scenarios is achieved as illustrated in Fig. 6. Each transition from the operating state i to j, which is realized
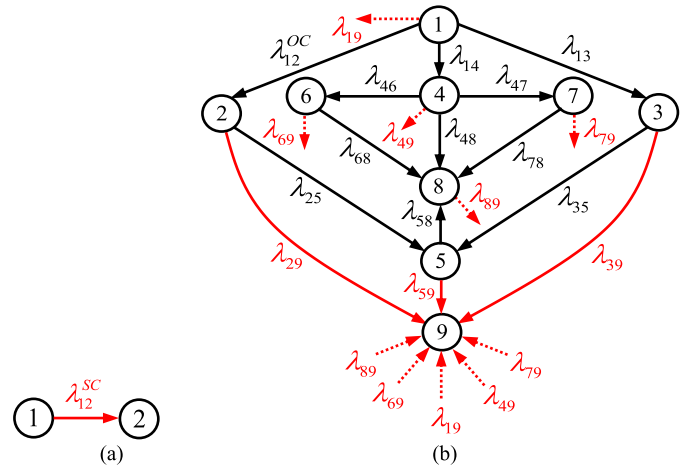

Fig. 6. Markov chain structure of the proposed converter under (a) SC and (b) OC fault scenarios.

due to a faulted component, is attributed a failure rate (λ_{ij}). Operating states 2 and 9 are found as the absorbing operating states under SC and OC fault scenarios, respectively. According to Fig. 6(a), the only one failure rate (λ_{12}^{SC}) under SC fault scenarios is assessed as the summation of all failure rates of converter components under SC fault scenarios and formulated as follows:

$$\lambda_{12}^{SC} = \lambda_{S1}^{SC} + \lambda_{S2}^{SC} + \lambda_{S3}^{SC} + \lambda_{Do1}^{SC} + \lambda_{Do2}^{SC} + \lambda_{Cr1}^{SC}$$
$$+ \lambda_{Cr2}^{SC} + \lambda_{\text{Trans}}^{SC} + \lambda_{Co}^{SC} \tag{23}$$

where the parameters are corresponded to the failure rates of the switches, the output diodes, the resonant and output capacitors, and the transformer under SC fault scenarios. As one can observe from Table II and Fig. 6(b), different λ_{ij} exist for the proposed converter as different operating states are projected under OC fault scenarios. Assuming the occurrence of SC faults, the SC-centered state-space equation is formulated as follows:

$$d/dt \begin{bmatrix} P_1^{\text{SC}}(t) & P_2^{\text{SC}}(t) \end{bmatrix} = \begin{bmatrix} P_1^{\text{SC}}(t) & P_2^{\text{SC}}(t) \end{bmatrix} \begin{bmatrix} -\lambda_{12}^{\text{SC}} & \lambda_{12}^{\text{SC}} \\ 0 & 0 \end{bmatrix} \tag{24}$$

where $P_1^{\text{SC}}(t)$ and $P_2^{\text{SC}}(t)$ are the probabilities of operating states 1 and 2 under SC fault scenarios. Considering the fact that the converter is on a healthy operating state at the beginning of its operation, the initial value for these probabilities are equal to

$$[P_{SC}(0)] = \begin{bmatrix} 1 & 0 \end{bmatrix}. \tag{25}$$

Since the operating state 2 is found to be the absorbing state under SC faults, the reliability of the proposed converter in such scenarios is equal to the probability of the first state as follows:

$$R_{\text{SC}}(t) = P_1^{\text{SC}}(t) = e^{-\lambda_{12}^{\text{SC}} t}. \tag{26}$$

TABLE III
IMPACTFUL FACTORS ON THE COMPONENTS FAILURE RATES

Component	Effective factors
Switch	$\lambda_S = \lambda_b \pi_T \pi_A \pi_Q \pi_E$
Diode	$\lambda_D = \lambda_b \pi_T \pi_S \pi_C \pi_Q \pi_E$
Transformer	$\lambda_{Trans} = \lambda_b \pi_T \pi_Q \pi_E$
Capacitor	$\lambda_C = \lambda_b \pi_T \pi_v \pi_Q \pi_E \pi_{SR} \pi_{Cap}$

On the other hand, the state-space equation under OC fault scenarios on the converter components is formulated as follows:

$$d/dt \left[P_1^{OC}(t) \quad P_2^{OC}(t) \quad \dots \quad P_9^{OC}(t) \right]$$

$$= \left[P_1^{OC}(t) \quad P_2^{OC}(t) \quad \dots \quad P_9^{OC}(t) \right] \times [\mathbf{M}] \quad (27)$$

where $P_1^{OC}(t) - P_9^{OC}(t)$ are the probabilities corresponding to the operating states 1–9 under OC fault scenarios, respectively, and $[\mathbf{M}]$ is equal to

$$\mathbf{M} =$$

$$\begin{bmatrix}
-k_1 & \lambda_{12} & \lambda_{13} & \lambda_{14} & 0 & 0 & 0 & 0 & \lambda_{19} \\
0 & -k_2 & 0 & 0 & \lambda_{25} & \lambda_{26} & 0 & 0 & \lambda_{29} \\
0 & 0 & -k_3 & 0 & \lambda_{35} & 0 & \lambda_{37} & 0 & \lambda_{39} \\
0 & 0 & 0 & -k_4 & 0 & \lambda_{46} & \lambda_{47} & 0 & \lambda_{49} \\
0 & 0 & 0 & 0 & -k_5 & 0 & 0 & \lambda_{58} & \lambda_{59} \\
0 & 0 & 0 & 0 & 0 & -k_6 & 0 & \lambda_{68} & \lambda_{69} \\
0 & 0 & 0 & 0 & 0 & 0 & -k_7 & \lambda_{78} & \lambda_{79} \\
0 & 0 & 0 & 0 & 0 & 0 & 0 & -k_8 & \lambda_{89} \\
0 & 0 & 0 & 0 & 0 & 0 & 0 & 0 & 0
\end{bmatrix}$$

$$(28)$$

where k_i is equal to the summation over all failure rates in row i, as the sum of all elements in each row of the matrix $\mathbf{M}$ must be zero. Similar to (25), the initial state probability under OC fault scenarios is assumed as follows:

$$[P_{OC}(0)] = \begin{bmatrix} 1 & 0 & \dots & 0 \end{bmatrix}. \quad (29)$$

As illustrated in Fig. 6(b), the operating state 9 is the absorbing state under OC faults. Hence, the reliability of the proposed converter under such scenarios is assessed as follows:

$$R_{OC}(t) = \sum_{i=1}^{8} P_i^{OC}(t). \quad (30)$$

In order to evaluate the failure rates of the converter components, Table III presents different factors that influence the failure rates, including the components' design quality (π_Q), environmental conditions (π_E), application factor (π_A), construction factor (π_C), series resistance factor (π_{SR}), and capacity factor (π_{Cap}) [25], [26]. In this article, we reasonably selected $\pi_Q = 8$, $\pi_E = 1$, $\pi_A = 8$, and $\pi_C = 1$ for the proposed converter [28], [29]. Furthermore, the electrical stress factor of a diode (π_S) and voltage stress factor of a capacitor (π_V) are

enforced as follows:

$$\pi_S = V_S^{2.43} \quad (31)$$

$$\pi_V = \left(\frac{S}{0.6} \right)^3 \qu(32)$$

where V_S is the voltage stress ratio and is defined as the ratio of the applied reverse voltage to the rated reverse voltage across the diode. Furthermore, S is the ratio of the operating voltage to the rated voltage across the capacitor.

Another important factor affecting the components' failure rates is the temperature (π_T), directly driven by the power loss of the equipment (P_S^{Loss}, P_D^{Loss}, and P_{Trans}^{Loss}). Table IV presents the key equations to characterize the temperature factor impacts on the equipment failure rates, where T_J, T_C, T_{HS}, T_A, and ΔT are the junction temperature, case temperature of switches and diodes, hot spot temperature of the transformer, ambient temperature, and average temperature rise above the ambient temperature, respectively. T_S is the switching period ($T_S = 2T$ s) and A is the case radiating surface area of the transformer (in^2). $R_{\theta JC}$ and $R_{\theta CA}$ (°C/W) are junction to case and case to ambient thermal resistances, respectively. According to [28], temperature factor of the capacitors depends on the ambient temperature, where it has a constant value of $\pi_T = 1.04$ under a constant ambient temperature. Table V summarizes the parameter values.

We utilized converter components in this study, which are all acquired from the available datasheets of IRFP260N, IRFP460N, and MUR1560. Eventually, numerical results presented in Table VI introduce the evaluated failure rates under SC and OC fault scenarios. The results presented in Table VI are further harnessed to evaluate the operating state probabilities under OC fault scenarios as tabulated in Table VII. Accordingly, the reliability metric of the proposed converter under SC and OC fault scenarios are assessed as follows:

$$R_{SC}(t) = e^{-151.78t} \quad (33)$$

$$R_{OC}(t) = -1.42e^{-151.78t} + 2.1e^{-98.78t}$$
$$- 0.56e^{-59.09t} + 1.25 \times 10^{-3}e^{-169.26t}$$
$$- 0.44e^{-47.72t} + 0.01e^{-94.57t} + 1.31e^{-47.67t}. \quad (34)$$

Furthermore, the MTTF index of reliability for the proposed converter under SC and OC fault scenarios is calculated as follows:

$$\text{MTTF}_{SC} = \int_0^\infty R_{SC}(t)dt = 6.6 \times 10^3 \text{ h} \quad (35)$$

$$\text{MTTF}_{OC} = \int_0^\infty R_{OC}(t)dt = 39.5 \times 10^3 \text{ h}. \quad (36)$$

Eventually, the overall system reliability and MTTF of the proposed converter topology are achieved as follows:

$$R(t) = aR_{SC}(t) + (1-a)R_{OC}(t) \quad (37)$$

TABLE IV
EVALUATION OF THE TEMPERATURE FACTOR ON THE CONVERTER COMPONENTS' FAILURE RATES [28], [29].

Component	Circuit Model	Power Loss	Junction and Hot Spot Temperatures	Temperature Factor
Switch	$R_{DS,on}$, i_S	$P_S^{Loss} = \frac{1}{T_S}\left[\int_0^{T_S} R_{DS,on}i_S^2(t)dt\right] + \left[C_\circ f_S V_S^2\right]$	$\begin{cases} T_J = T_C + R_{\theta JC}P_S^{Loss} \\ T_C = T_A + R_{\theta CA}P_S^{Loss} \end{cases}$	$\pi_T = \exp\left[-1925(\frac{1}{T_J+273} - \frac{1}{298})\right]$
Diode	V_f, R_D, i_D	$P_D^{Loss} = \frac{1}{T_S}\left[\int_0^{T_S}\left(R_D i_D^2(t) + V_f i_D(t)\right)dt\right]$	$\begin{cases} T_J = T_C + R_{\theta JC}P_D^{Loss} \\ T_C = T_A + R_{\theta CA}P_D^{Loss} \end{cases}$	$\pi_T = \exp\left[-3091(\frac{1}{T_J+273} - \frac{1}{298})\right]$
Transformer	R_{Trans}, i_{Trans}	$P_{Trans}^{Loss} = \frac{1}{T_S}\left[\int_0^{T_S} R_{Trans}i_{Trans}^2(t)dt\right]$	$\begin{cases} T_{HS} = T_A + 1.2\Delta T \\ \Delta T = \dfrac{125P_{Trans}^{Loss}}{A} \end{cases}$	$\pi_T = \exp\left[\dfrac{-0.11}{8.617\times10^{-5}}(\frac{1}{T_{HS}+273} - \frac{1}{298})\right]$

Note: All temperature factors are in degrees centigrade.

TABLE V
ESSENTIAL PARAMETERS AND SELECTED VALUES FOR FAILURE
RATE ASSESSMENTS

Components	Parameters and Values
S_1 and S_2	$R_{DS,on} = 0.04\Omega$, $C_o = 603pF$, $R_{\theta JC} = 0.5\,°C/W$, $R_{\theta CA} = 40.5\,°C/W$ and $\lambda_b = 0.06$
S_3	$R_{DS,on} = 0.27\Omega$, $C_o = 870pF$, $R_{\theta JC} = 0.5\,°C/W$, $R_{\theta CA} = 40.5\,°C/W$ and $\lambda_b = 0.06$
D_{o1} and D_{o2}	$V_f = 1.5V$, $R_D = 0.02\Omega$, $R_{\theta JC} = 2\,°C/W$, $R_{\theta CA} = 62\,°C/W$ and $\lambda_b = 0.0038$
C_{r1}, C_{r2} and C_o	$\lambda_b = 0.002$
Transformer ($Trans$)	$R_{Trans} = 0.038\Omega$, $A = 0.22in^2$ and $\lambda_b = 0.049$

Note: λ_b is in failures per 10^6 h.

TABLE VI
CALCULATED FAILURE RATES UNDER SC AND OC FAULT SCENARIOS

Parameter	Value	Parameter	Value	Parameter	Value
λ_{12}^{SC}	151.78	λ_{29}	89.21	λ_{58}	0.076
λ_{12}^{OC}	137.56	λ_{35}	58.22	λ_{59}	47.46
λ_{13}	12.52	λ_{37}	0.036	λ_{68}	23.6
λ_{14}	0.036	λ_{39}	0.83	λ_{69}	70.97
λ_{19}	1.66	λ_{46}	137.56	λ_{78}	58.22
λ_{25}	9.52	λ_{47}	30	λ_{79}	0.87
λ_{26}	0.036	λ_{49}	1.7	λ_{89}	47.67

Note: All failure rates are in failures per 10^6 h.

$$\text{MTTF} = \int_0^\infty R(t)dt = a\cdot\text{MTTF}_{\text{SC}} + (1-a)\cdot\text{MTTF}_{\text{OC}} \tag{38}$$

where a is the probability of SC fault occurrence. Employing (37) and (38), a sensitivity analysis on different selections of a and the impacts on the reliability and MTTF metrics is provided in Fig. 7. In Fig. 7(a), the reliability performance is presented with respect to time duration, and in Fig. 7(b),
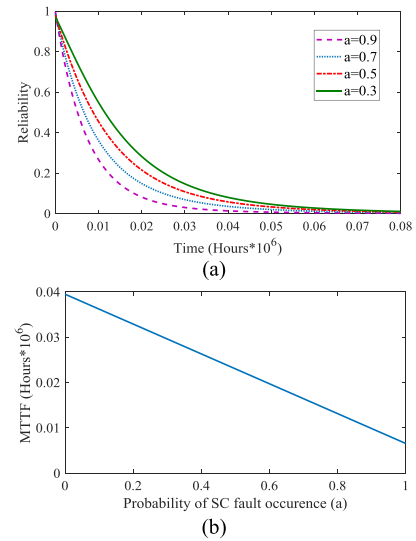

Fig. 7. Reliability and MTTF metrics with different selections of a. (a) Reliability versus time. (b) MTTF versus a.

MTTF is illustrated with respect to a. One can see from Fig. 7 that with the increase in a, the converter reliability and MTTF decrease primarily driven by the absorbing states under all SC fault scenarios.

In order to further verify the reliability performance of the proposed converter against other topologies, a comparison is made with its full-bridge topology in Fig. 8 for $a = 0.9$ and $a = 0.7$. The proposed converter reveals a higher reliability performance than that by its full-bridge topology, the reasons for which are twofold. First, the reliability performance decreases in series combination of components, where a fault on one will result in a total system failure. This combination exists in the full-bridge converter, when two switches are simultaneously turned ON in series. Second, a full-bridge topology has two additional primary-side switches with half voltage stress and the same current flowing through, and compared to the proposed push–pull converter, generates a high switch conduction power loss particularly under a higher transformer turns ratio. It can be concluded from the presented results that the switches (with high failure rates) are the most critical components in power electronic converters affecting the system reliability the most.

TABLE VII
OPERATING STATE PROBABILITIES UNDER OC FAULT SCENARIOS [30]

| Operating States	Probabilities	Numerical Results
$P_1^{OC}(t)$	$e^{-k_1 t}$	$e^{-151.78t}$
$P_2^{OC}(t)$	$\dfrac{\lambda_{12}^{OC}}{k_2 - k_1}(e^{-k_1 t} - e^{-k_2 t})$	$2.59(e^{-98.78t} - e^{-151.78t})$
$P_3^{OC}(t)$	$\dfrac{\lambda_{13}}{k_3 - k_1}(e^{-k_1 t} - e^{-k_3 t})$	$0.13(e^{-59.08t} - e^{-151.78t})$
$P_4^{OC}(t)$	$\dfrac{\lambda_{14}}{k_4 - k_1}(e^{-k_1 t} - e^{-k_4 t})$	$2.06 \times 10^{-3}(e^{-151.78t} - e^{-169.26t})$
$P_5^{OC}(t)$	$X_1 e^{-k_1 t} + X_2 e^{-k_2 t} + X_3 e^{-k_3 t} + X_4 e^{-k_5 t}$	$0.3e^{-151.78t} - 0.48e^{-98.78t} - 0.69e^{-59.08t} + 0.87e^{-47.72t}$
$P_6^{OC}(t)$	$X_5 e^{-k_1 t} + X_6 e^{-k_2 t} + X_7 e^{-k_4 t} + X_8 e^{-k_6 t}$	$-3.32 \times 10^{-3} e^{-151.78t} - 0.02e^{-98.78t} + 3.79 \times 10^{-3} e^{-169.26t} + 0.02e^{-94.57t}$
$P_7^{OC}(t)$	$X_9 e^{-k_1 t} + X_{10} e^{-k_3 t} + X_{11} e^{-k_4 t} + X_{12} e^{-k_7 t}$	$-4.9 \times 10^{-3} e^{-151.78t} + 1.21e^{-59.08t} + 5.61 \times 10^{-4} e^{-169.26t} - 1.21e^{-59.09t}$
$P_8^{OC}(t)$	$(X_{13} + X_{14} + X_{15})e^{-k_1 t} + X_{16} e^{-k_2 t} + X_{17} e^{-k_3 t} + X_{18} e^{-k_4 t} + X_{19} e^{-k_5 t} + X_{20} e^{-k_6 t} + X_{21} e^{-k_7 t} + (X_{22} + X_{23} + X_{24})e^{-k_8 t}$	$1.8 \times 10^{-3} e^{-151.78t} + 0.01e^{-98.78t} + 4.1 \times 10^{-3} e^{-59.09t} - 1.04 \times 10^{-3} e^{-169.26t} - 1.31e^{-47.72t} - 0.01e^{-94.57t} + 1.31e^{-47.67t}$
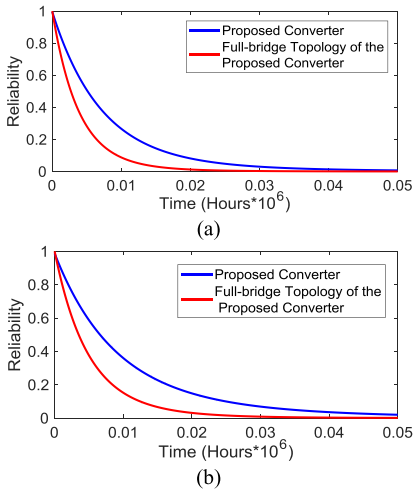
Fig. 8. Reliability performance comparison of the proposed converter and its full-bridge topology. (a) $a = 0.9$. (b) $a = 0.7$.
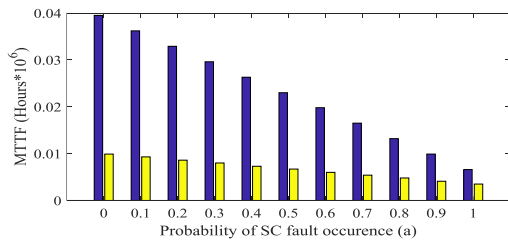

Fig. 9. MTTF comparison of the proposed converter (blue) and its full-bridge topology (yellow) with different values of a.

Fig. 10. Reliability comparison of the proposed converter with other soft switching push–pull converters in two scenarios. (a) $P_o = 100$ W and $a = 0.7$. (b) $P_o = 250$ W and $a = 0.8$.

can see in Fig. 9 that the MTTF of the proposed converter and its full-bridge structure will differ significantly as a decreases.

In Fig. 10, reliability of the proposed converter is compared with the reliability of other dc–dc push–pull converters under different operating conditions ($P_o = 100$ W and $a = 0.7$) and ($P_o = 250$ W and $a = 0.8$). According to Fig. 10, the following statements hold.

1) The proposed converter offers the highest reliability performance in both operating conditions.

We also compared the MTTF index of reliability for the proposed converter with its full-bridge topology in Fig. 9. The presented results in Fig. 9 verify the observations in Fig. 8. One
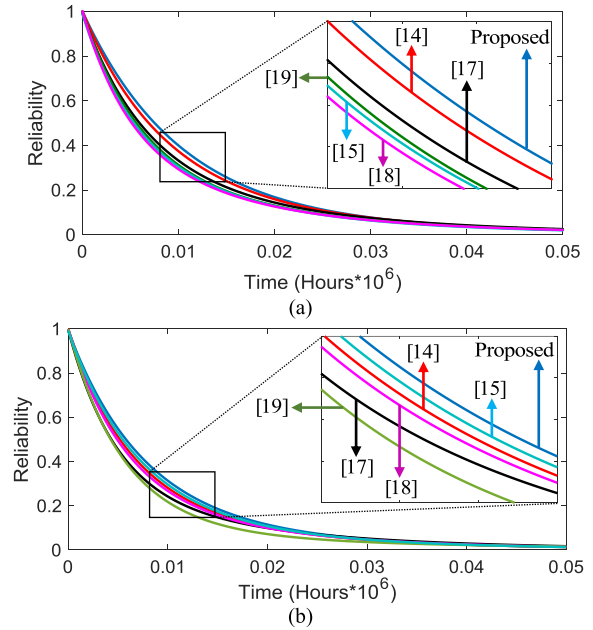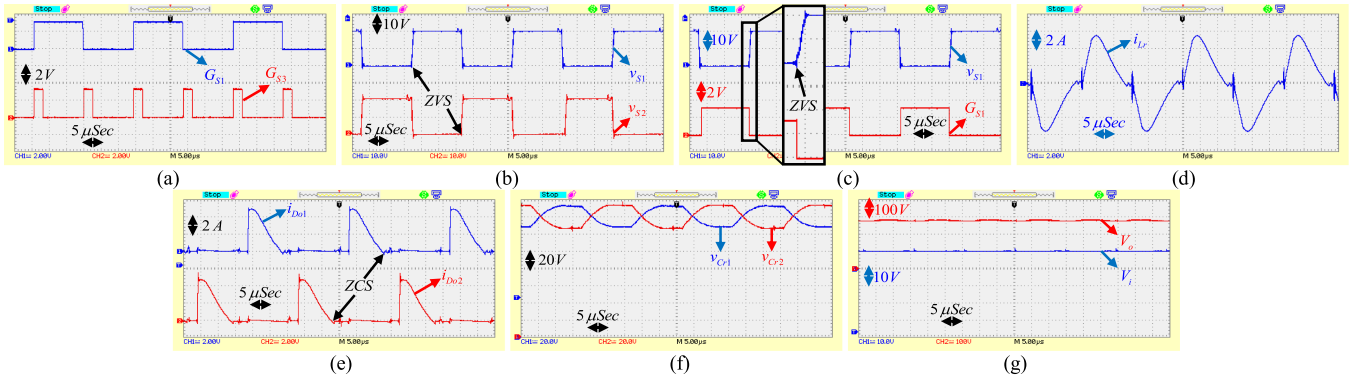
Fig. 11.   Experimental results of the proposed soft switching push–pull dc–dc converter: general observations.
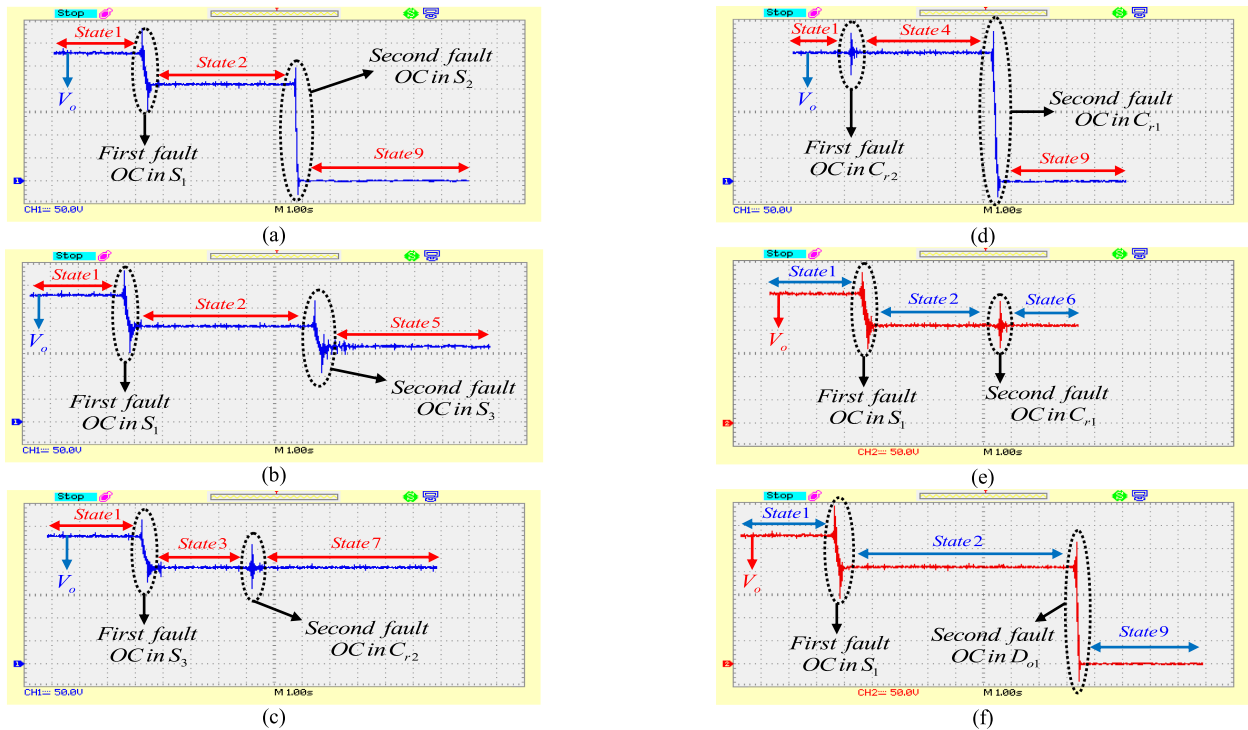

Fig. 12.   Experimental test of the proposed converter under different OC fault scenarios. (a) S_1 and S_2. (b) S_1 and S_3. (c) S_3 and C_{r2}. (d) C_{r2} and C_{r1}. (e) S_1 and C_{r1}. (f) S_1 and D_{o1}.

2) Variations in P_o and a affect the converters reliability differently; for instance, when the output power P_o decreases from 250 to 100 W, the reliability performance increases in the case of the proposed converter, whereas it is the reverse in converter topologies presented in [15] and [18].

3) The rate of reliability degradation is different among the compared converters.

V. EXPERIMENTAL RESULTS

In order to verify the performance of the proposed dc–dc converter topology under real-world operating conditions, several experimental tests are performed, the results of which are presented in Fig. 11. The test setup is characterized with $L_m = 7.27$ mH, $L_r = 108$ μH, $C_r = 0.33$ μF, $n = 12.5$, and the switching frequency of 34.7 kHz. In this experimental test, IRFP260N, IRFP460N, and MUR1560 are employed as the primary-side switches, secondary-side switches, and the output diodes, respectively. The experimental test results on the proposed converter are achieved with $V_i = 10$ V and $V_o = 280$ V.

Fig. 11(a) illustrates the applied gate pulses to the switches. In Fig. 11(b), the voltage across the primary-side switches are demonstrated, with the maximum value of $2V_i = 20$ V observed when in turn-OFF modes. These switches are commutated under the ZVS conditions in the short-interval modes of 4 and 8. In order to further verify the ZVS operation, Fig. 11(c) conjointly illustrates the voltage and the gate pulse across the S_1 switch. In Fig. 11(d), i_{Lr} is depicted, revealing linear and sinusoidal
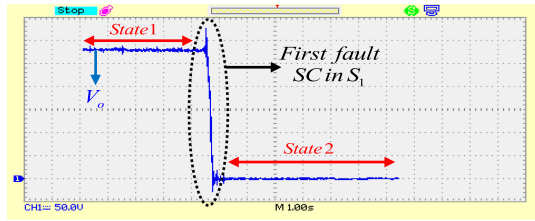
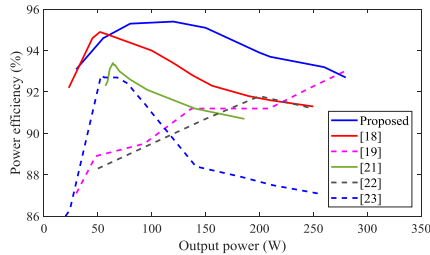Fig. 13. Experimental test of the proposed converter under an SC fault on S_1.

Fig. 14. Converter power efficiency with respect to the output power.

compared. The reliability and MTTF evaluations of the proposed converter under both SC and OC fault scenarios were evaluated. Assessments of components failure rates in different operating states were pursued centered on the Markov process principles. Under a SC fault probability of 70%, the converter MTTF was calculated as 16.5×10^3 h. Moreover, a 280-W prototype with input voltage of 10 V, output voltage of 280 V, and switching frequency of 34.7 kHz was developed that could experimentally verify the accuracy of the discussed theoretical analysis and simulation results.

The proposed analytics in this article provided insights that can help making informative decisions in designing and implementing a more reliable power electronic converter in industrial applications. With detailed theoretical, operational, and experimental analysis, the proposed soft switching push–pull dc–dc converter offers a promising operational reliability performance in many practical settings and under a wide range of real-world scenarios, including, but not limited to, open circuit faults on various components and multiple derated operating states.

waveforms in modes 1 and 2, respectively. In Fig. 11(e), v_{Do1} and v_{Do2} are presented with $180°$ phase shift when the ZCS turned OFF. In Fig. 11(f), v_{Cr1} and v_{Cr2}, with the average values of $V_o/2$ and a phase shift of $180°$, are demonstrated, reflecting a resonant operation in modes 2 and 6. In Fig. 11(g), the input and output voltages in the proposed push–pull converter are presented. The results in Fig. 11(g) validate the promising capability of the proposed converter in constantly generating a regulated output voltage with a reasonably high voltage gain.

Additionally, we experimentally verify the claimed performance of the proposed converter in its derated operating states and under different output power scenarios. Figs. 12 and 13 demonstrate the experimental observations when different OC and SC fault scenarios are applied on various converter elements. The operating states numbered in these figures correspond to details provided in Fig. 5 and Table II.

Fig. 14 compares the power efficiency of the proposed converter with the power efficiency of other soft switching push–pull converters, indeed with the same components characteristics. According to Fig. 14, the proposed converter offers an acceptably high efficiency in comparison with other similar converters. The maximum power efficiency of the proposed converter is 95.4%, which is achieved when $P_o = 121$ W.

VI. CONCLUSION

A new soft switching isolated push-pull dc–dc converter was proposed in this article, assembling a push–pull structure in the primary side, a capacitive voltage doubler in the secondary side, and a three-winding transformer in between. Through a simple resonant tank and a bidirectional switch, the suggested topology offered ZVS for the primary-side switches with low switching currents and ZCS for the secondary-side diodes. A comprehensive analysis of the proposed converter with ideal steady-state waveforms, under different component design characteristics and soft switching capability, were conducted and extensively

REFERENCES

[1] Y. Azadeh, E. Babaei, H. Tarzamni, and M. Sabahi, "Single-inductor dual-output DC/DC converter with capability of feeding a constant power load in open-loop manner," *IEEE Trans. Ind. Electron.*, vol. 66, no. 9, pp. 6906–6915, Sep. 2019.

[2] A. Dehghanzadeh, Gh. Farahani, H. Vahedi, and K. Al-Haddad, "Model predictive control design for DC-DC converters applied to a photovoltaic system," *Int. J. Elect. Power Energy Syst.*, vol. 103, pp. 537–544, 2018.

[3] H. Trazamni, E. Babaei, and M. Sabahi, "Full soft-switching high step-up DC–DC converter based on active resonant cell," *IET Power Electron.*, vol. 10, no. 13, pp. 1729–1739, 2017.

[4] J. W. Kim and J. I. Ha, "Dual voltage regulations of single switch flyback converter using variable switching frequency," in *Proc. IEEE Appl. Power Electron. Conf. Expo.*, 2016, pp. 1398–1402.

[5] Y. Panov and M. M. Jovanovic, "Adaptive off-time control for variablefrequency, soft-switched flyback converter at light loads," *IEEE Trans. Power Electron.*, vol. 17, no. 4, pp. 596–603, Jul. 2002.

[6] T. LaBella, B. York, C. Hutchens, and J. S. Lai, "Dead time optimization through loss analysis of an active-clamp flyback converter utilizing GaN devices," in *Proc. IEEE Energy Convers. Congr. Expo.*, 2012, pp. 3882–3889.

[7] H. Tarzamni, E. Babaei, and A. Zarrin Gharehkoushan, "A full soft-switching ZVZCS flyback converter using an active auxiliary cell," *IEEE Trans. Ind. Electron.*, vol. 64, no. 2, pp. 1123–1129, Feb. 2017.

[8] J. Sun, X. Ding, M. Nakaoka, and H. Takano, "A novel series resonant ZCS full bridge three-level dc–ac inverter," in *Proc. IEEE 21st Annu. IEEE Appl. Power Electron. Conf. Expo.*, 2008, pp. 419–425.

[9] W. Chen, Y. Gu, and Z. Lu, "A novel three Level full bridge resonant dc–dc converter suitable for high power wide range input applications," in *Proc. IEEE 22nd Annu. IEEE Appl. Power Electron. Conf. Expo.*, 2007, pp. 373–379.

[10] X. Zhang, H. Chung, X. Ruan, and A. Ioinovici, "A ZCS full-bridge converter without voltage overstress on the switches," *IEEE Trans. Power Electron.*, vol. 25, no. 3, pp. 686–698, Mar. 2010.

[11] B. Yang, F. C. Lee, A. J. Zhang, and G. Huang, "LLC resonant converter for front end DC/DC conversion," in *Proc. 17th Annu. IEEE Appl. Power Electron. Conf. Expo.*, 2002, pp. 1108–1112.

[12] F. Musavi, M. Craciun, D. S. Gautam, W. Eberle, and W. G. Dunford, "An LLC resonant DC–DC converter for wide output voltage range battery charging applications," *IEEE Trans. Power Electron.*, vol. 28, no. 12, pp. 5437–5445, Dec. 2013.

[13] H. Hu, X. Fang, F. Chen, Z. J. Shen, and I. Batarseh, "A modified high efficiency LLC converter with two transformers for wide input-voltage range applications," *IEEE Trans. Power Electron.*, vol. 28, no. 4, pp. 1946–1960, Apr. 2013.

[14] I. Boonyaroonate and S. Mori, "A new ZVCS resonant push-pull DC/DC converter topology," in *Proc. 17th Annu. IEEE Appl. Power Electron. Conf. Expo.*, 2002, pp. 1097–1100.

[15] C. L. Chu and C. H. Li, "Analysis and design of a current-fed zero-voltage-switching and zero-current-switching CL-resonant push-pull dc-dc converter," *IET Power Electron.*, vol. 2, no. 4, pp. 456–465, Jul. 2009.

[16] M. J. Ryan, W. E. Brumsickle, D. M. Divan, and R. D. Lorenz, "A new ZVS LCL-resonant push-pull DC-DC converter topology," *IEEE Trans. Ind. Appl.*, vol. 34, no. 5, pp. 1164–1174, Sep./Oct. 1998.

[17] J. Ying, Q. Zhu, H. Lin, and Z. Wu, "A zero-voltage-switching (ZVS) push-pull DC/DC converter for UPS," in *Proc. 5th Int. Conf. Power Electron. Drive Syst.*, 2003, vol. 2, pp. 1495–1499.

[18] P. Xuewei and A. K. Rathore, "Naturally clamped zero-current commutated soft-switching current-fed push–pull DC/DC converter: analysis, design, and experimental results," *IEEE Trans. Power Electron.*, vol. 30, no. 3, pp. 1318–1327, Mar. 2015.

[19] S. Bal, A. K. Rathore, and D. Srinivasan, "Naturally clamped snubberless soft-switching bidirectional current-fed three-phase push-pull DC/DC converter for DC micro-grid application," in *Proc. IEEE Appl. Power Electron. Conf. Expo.*, 2015, pp. 717–724.

[20] P. Xuewei and A. K. Rathore, "Naturally commutated and clamped soft-switching current-fed push-pull voltage doubler based solar PV inverter," in *Proc. IEEE 23rd Int. Symp. Ind. Electron.*, 2014, pp. 2631–2636.

[21] F. H. Aghdam and M. Abapour, "Reliability and cost analysis of multistage boost converters connected to PV panels," *IEEE J. Photovolt.*, vol. 6, no. 4, pp. 981–989, Jul. 2016.

[22] A. Khosroshahi, M. Abapour, and M. Sabahi, "Reliability evaluation of conventional and interleaved DC–DC boost converters," *IEEE Trans. Power Electron.*, vol. 30, no. 10, pp. 5821–5828, Oct. 2015.

[23] H. Tarzamni, E. Babaei, A. Zarrin Gharehkoushan, and M. Sabahi, "Interleaved full ZVZCS DC–DC boost converter: Analysis, design, reliability evaluations and experimental results," *IET Power Electron.*, vol. 10, no. 7, pp. 835–845, 2017.

[24] H. Tarzamni, F. Tahami, M. Fotuhi-Firuzabad, and F. P. Esmaeelnia, "Reliability analysis of buck-boost converter considering the effects of operational factors," in *Proc. 10th Int. Power Electron., Drive Syst. Technol. Conf.*, 2019, pp. 647–652.

[25] J. Lee, J. Kwon, E. Kim, and B. Kwon, "Dual series-resonant active-clamp converter," *IEEE Trans. Ind. Electron.*, vol. 55, no. 2, pp. 699–710, Feb. 2008.

[26] S. Chen, T. Liang, L. Yang, and J. Chen, "A safety enhanced, high step-up DC–DC converter for AC photovoltaic module application," *IEEE Trans. Power Electron.*, vol. 27, no. 4, pp. 1809–1817, Apr. 2012.

[27] F. Abbasi Aghdam Meinagh, E. Babaei, and H. Tarzamni, "Modified high voltage gain switched boost inverter," *IET Power Electron.*, vol. 10, no. 13, pp. 1655–1664, Oct. 2017.

[28] U.S. Department of Defense, *Military Handbook—Reliability Prediction of Electronic Equipment*, MIL-HDBK-217F, 1991.

[29] "RIAC-MIL-HDBK-217Plus, Reliability Prediction Models," Reliability Information Analysis Center, Utica, NY, USA, 2006.

[30] R. Billinton and R. N. Allan, *Reliability Evaluation of Engineering Systems, Concepts and Techniques*, 2nd ed. New York, NY, USA: Springer, 1992.

Hadi Tarzamni (S'18) was born in Tabriz, Iran, in 1992. He received the B.Sc. (Hons.) and M.Sc. (Hons.) degrees in power electrical engineering from the Faculty of Electrical and Computer Engineering, University of Tabriz, Tabriz, Iran, in 2014 and 2016, respectively. He is currently working toward the Ph.D. degree in power electronics engineering with the Department of Electrical Engineering, Sharif University of Technology, Tehran, Iran.

His research interests include power electronic converters analysis and design, dc–dc converters, soft-switching and resonant converters, and reliability analysis.

Ebrahim Babaei (M'10–SM'16) received the Ph.D. degree in electrical engineering from the University of Tabriz, Tabriz, Iran, in 2007.

In 2007, he joined the Faculty of Electrical and Computer Engineering, University of Tabriz. He is the author and coauthor of more than 480 journal and conference papers. He also holds 25 patents in the area of power electronics. His current research interests include the analysis, modeling, design, and control of power electronic converters and their applications, renewable energy sources, and FACTS devices.

Farhad Panahandeh Esmaeelnia was born in Tabriz, Iran, in 1993. He received the B.Sc. and M.Sc. degrees in power electrical engineering from the Faculty of Electrical and Computer Engineering, University of Tabriz, Tabriz, Iran, in 2015 and 2017, respectively.

His research interests include reliability analytics of power electronic converters.

Payman Dehghanian (S'11–M'17) received the B.Sc. degree in electrical engineering from the University of Tehran, Tehran, Iran, in 2009, the M.Sc. degree in electrical engineering from the Sharif University of Technology, Tehran, Iran, in 2011, and the Ph.D. degree in electrical engineering from Texas A&M University, College Station, Texas, USA, in 2017.

He is currently an Assistant Professor with the Department of Electrical and Computer Engineering, George Washington University, Washington, DC, USA. His research interests include power system protection and control, and power system reliability and resiliency.

Sajjad Tohidi was born in Meshkin Shahr, Iran, in 1984. He received the B.Sc. degree from the Iran University of Science and Technology, Tehran, Iran, in 2006, and the M.Sc. and Ph.D. degrees from Sharif University of Technology, Tehran, Iran, in 2008, and 2012, respectively, all in electrical engineering.

He is currently an Associate Professor with the Faculty of Electrical and Computer Engineering, University of Tabriz, Tabriz, Iran. His research interests include electrical machines.

Mohammad Bagher Bannae Sharifian received the B.Sc. and M.Sc. degrees in electrical engineering from the University of Tabriz, Tabriz, Iran, in 1989 and 1992, respectively, and the Ph.D. degree in electrical engineering from the University of Tabriz, in 2000.

In 2000, he rejoined as an Assistant Professor with the Electrical Power Department, Faculty of Electrical and Computer Engineering, University of Tabriz, where he is currently a Professor. His research interests include modeling and analysis of electrical machines.